Article

Thermodynamics Analysis of Variable Viscosity Hydromagnetic Couette Flow in a Rotating System with Hall Effects

Oluwole D. Makinde [1,†], Adetayo S. Eegunjobi [2,†,*] and M. Samuel Tshehla [1,†]

[1] Faculty of Military Science, Stellenbosch University, Private Bag X2, Saldanha 7395, South Africa;
E-Mails: makinded@gmail.com (O.D.M.); sammietshehla@gmail.com (M.S.T.)

[2] Department of Mathematics and Statistics, Namibia University of Science and Technology,
Private Bag 13388, 13 Storch street, Windhoek, Namibia

[†] These authors contributed equally to this work.

[*] Author to whom correspondence should be addressed; E-Mail: samdet1@yahoo.com;
Tel.: +264-61-207-2536.

Academic Editor: Kevin H. Knuth

Abstract: In this paper, we employed both first and second laws of thermodynamics to analyze the flow and thermal decomposition in a variable viscosity Couette flow of a conducting fluid in a rotating system under the combined influence of magnetic field and Hall current. The non-linear governing differential equations are obtained and solved numerically using shooting method coupled with fourth order Runge–Kutta–Fehlberg integration technique. Numerical results obtained for velocities and temperature profiles are utilized to determine the entropy generation rate, skin fictions, Nusselt number and the Bejan number. By plotting the graphs of various values of thermophysical parameters, the features of the flow characteristics are analyzed in detail. It is found that fluid rotation increases the dominant effect of heat transfer irreversibility at the upper moving plate region while the entropy production is more at the lower fixed plate region.

Keywords: MHD couette flow; rotating system; variable viscosity; Hall effects; entropy analysis

1. Introduction

The flow of an electrically and thermal conducting fluid between two parallel plates in the presence of a transverse magnetic field do appear in a wide variety of industrial and engineering applications, as well as in many natural circumstances such as geothermal extraction, storage of nuclear waste material, oil recovery processes, thermal insulation engineering, pollutant dispersion in aquifers, food processing, casting and the dispersion of chemical contaminants in various processes in the chemical industry and in the environment, electromagnetic casting, astrophysics and cosmology, earthquake, magnetic drug targeting, magnetohydrodynamic (MHD) power generators, boundary layer flow control and MHD pumps. MHD flow in a rotating system is also encountered in geophysical fluid dynamics. It is well known that a number of astronomical bodies possess fluid interiors and magnetic fields. Changes that take place in the rate of rotation suggest the possible importance of hydromagnetic spin-up. Barikbin *et al.* [1] applied the Ritz–Galerkin method in Bernstein polynomial basis to solve the nonlinear problem of the magnetohydrodynamics (MHD) flow of third grade fluid between two plates. Khan *et al.* [2] investigated the peristaltic motion of an incompressible non-Newtonian fluid with variable viscosity through a porous medium in an inclined symmetric channel under the effect of slip condition. Hydromagnetic Couette flow subject to different physical effects, have been studied by many researchers [3–6]. Attia [7] studied the unsteady Couette–Poiseuille flow of an electrically conducting incompressible non-Newtonian viscoelastic fluid between two parallel horizontal non-conducting porous plates with heat transfer putting into consideration the Hall Effect. Makinde and Chinyoka [8] studied the unsteady hydromagnetic generalized Couette flow and heat transfer characteristics of a reactive variable viscosity incompressible electrically conducting third grade fluid in a channel with asymmetric convective cooling at the walls in the presence of uniform transverse magnetic field. Eegunjobi and Makinde [9] examined the effects of the thermodynamic second law on steady flow of an incompressible variable viscosity electrically conducting fluid in a channel with permeable walls and convective surface boundary conditions.

Many authors have investigated the fluid dynamic of rotating systems under various geometry due to its various applications such as compressor, wind turbine, jet engine, pumps, large-scale atmospheric and oceanic flows. Shivakumara *et al.* [10] studied the simultaneous effect of a vertical AC electric field and rotation on the onset of thermal convective instability in a horizontal rotating dielectric fluid layer by performing linear stability analysis. Nadeem and Saleem [11] investigated of third grade fluid flow over a rotating vertical cone in the presence of nanoparticles, *i.e.*, thermophoresis and Brownian motion. Turkyilmazoglu [12] investigated analytical solutions for the flow of a viscous hydromagnetic fluid due to the rotation of an infinite disk in the presence of an axial uniform steady magnetic field with the inclusion of Hall current effects and porosity. Zakinyan *et al.* [13] experimentally investigated the behavior of a magnetic fluid drop lying on a solid horizontal surface and surrounded by a nonmagnetic liquid under the action of a uniform magnetic field that is rotating in a vertical plane with low frequency. Feiz-Dizaji *et al.* [14] investigated the flow field of a third-grade non-Newtonian fluid in the annulus of rotating concentric cylinders in the presence of magnetic field. Hayat *et al.* [15] developed an exact solution to analyze an electrical conducting viscous fluid over a porous plate in a rotating system and many other works [16–18].

In this present study, both first and second laws of thermodynamics are employed to investigate the flow and thermal decomposition in hydromagnetic variable viscosity Couette flow in a rotating system with Hall current. The nonlinear model problem is tackled numerically using shooting technique coupled with fourth order Runge–Kutta–Fehlberg integration scheme. Results for both the primary and secondary velocity profiles, temperature profiles entropy generation rate, Bejan number, skin friction and Nusselt number are displayed graphically and discussed quantitatively.

2. Mathematical Analysis

Consider the steady Couette flow of a variable viscosity, incompressible, electrically and thermally conducting fluid between two infinite parallel walls $y = 0$ and $y = L$ in the presence of a uniform transverse magnetic field B_0 that is applied parallel to y-axis taking Hall current into account. Both the fluid and channel rotate in unison with a uniform angular velocity Ω about y-axis. The deflection effect of Coriolis force acting perpendicular to the direction of fluid motion and to the axis of rotating reference frame is considered while the effect of centrifugal force is negligible due to fluid axial Couette flow motion. Fluid flow within the channel is induced due to uniform pressure gradient applied along x-direction as well as the movement of upper wall $y = L$ with uniform velocity U_0 in the same direction. The walls of the channel are maintained at the same temperature T_w. Physical model of the problem is presented in Figure 1. Since channel walls are of infinite extent in x- and z-directions and the flow is fully developed, all physical quantities, except pressure depend on y only.
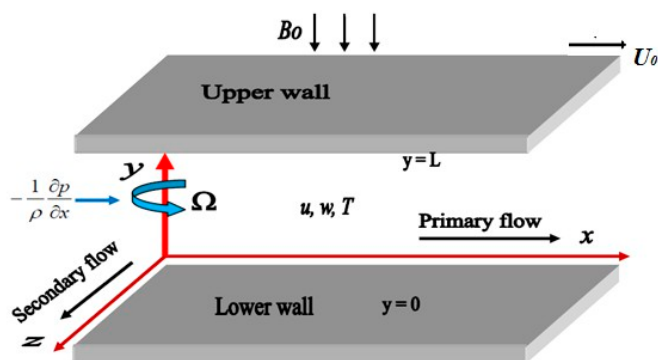

Figure 1. Physical model of the problem.

Taking into consideration the assumptions made above, the governing equations for steady Couette flow of a viscous, incompressible, electrically and thermally conducting fluid in a rotating system taking Hall current into account are presented in the following form [2–4,15,17]

$$2\Omega w = -\frac{1}{\rho}\frac{\partial P}{\partial x} + \frac{1}{\rho}\frac{\partial}{\partial y}\left(\mu\frac{\partial u}{\partial y}\right) - \frac{\sigma B_0^2 (u + mw)}{\rho(1+m^2)} \tag{1}$$

$$-2\Omega u = -\frac{1}{\rho}\frac{\partial P}{\partial z} + \frac{1}{\rho}\frac{\partial}{\partial y}\left(\mu\frac{\partial w}{\partial y}\right) - \frac{\sigma B_0^2 (w - mu)}{\rho(1+m^2)} \tag{2}$$

$$\frac{k}{\rho c_p}\frac{\partial^2 T}{\partial y^2} + \frac{\mu}{\rho c_p}\left[\left(\frac{\partial u}{\partial y}\right)^2 + \left(\frac{\partial w}{\partial y}\right)^2\right] + \frac{\sigma B_0^2}{\rho c_p}\left[\frac{(u - U_0 + mw)^2 + (w - mu + mU_0)^2}{(1+m^2)^2}\right] = 0 \tag{3}$$

$$E_g = \frac{k}{T_w^2}\left(\frac{\partial T}{\partial y}\right)^2 + \frac{\mu}{T_w}\left[\left(\frac{\partial u}{\partial y}\right)^2 + \left(\frac{\partial w}{\partial y}\right)^2\right] + \frac{\sigma B_0^2}{T_w}\left[\frac{(u - U_0 + mw)^2 + (w - mu + mU_0)^2}{(1 + m^2)^2}\right] \tag{4}$$

where $u, w, T, \sigma, \rho, m = \omega_e\tau_e, \omega_e, \tau_e, k, c_p$ and E_g are, respectively, the fluid velocity in *x*-direction, fluid velocity in *z*-direction, fluid temperature, fluid electrical conductivity, fluid density, Hall current parameter, cyclotron frequency, electron collision time, thermal conductivity coefficient, specific heat at constant pressure and the volumetric entropy generation rate. The boundary conditions for the fluid velocities and temperature are given as:

$$u(0) = 0, \qquad w(0) = 0, \qquad T(0) = T_w,$$
$$u(L) = U_0, \qquad w(L) = 0, \qquad T(L) = T_w. \tag{5}$$

Due to the movement of the upper plate, the pressure gradient terms $-\frac{1}{\rho}\frac{\partial P}{\partial x}$ and $-\frac{1}{\rho}\frac{\partial P}{\partial z}$, which are present in Equations (1) and (2), respectively, are evaluated with the help of Boundary Conditions (5) and are given by

$$-\frac{1}{\rho}\frac{\partial p}{\partial x} = \frac{\sigma B_0^2 U_0}{\rho(1 + m^2)}, \qquad -\frac{1}{\rho}\frac{\partial p}{\partial z} = -2\Omega U_0 - \frac{\sigma B_0^2 m U_0}{\rho(1 + m^2)} \tag{6}$$

The fluid dynamical viscosity is assumed to be an exponential decreasing function of temperature given by [3,9]

$$\mu(T) = \mu_0 e^{-\beta(T - T_w)} \tag{7}$$

where μ_0 is the fluid dynamic viscosity at the walls. We introduce the dimensionless variables and parameters as follows:

$$\eta = \frac{y}{L}, \ X = \frac{x}{L}, \ \theta = \frac{T - T_w}{T_w}, \ \delta = \beta T_w, \ \upsilon = \frac{\mu_0}{\rho}, \ U = \frac{uL}{\upsilon}, \ W = \frac{wL}{\upsilon}, \ \Pr = \frac{\mu_0 c_p}{k},$$
$$Ec = \frac{\upsilon^2}{c_p T_w L^2}, \ M = \frac{\sigma B_0^2 L^2}{\mu_0}, \ R_0 = \frac{\Omega L^2}{\upsilon}, \ Ns = \frac{E_g L^2}{k}, \ \lambda = \frac{U_0 L}{\upsilon}. \tag{8}$$

Substituting Equation (8) into Equations (1)–(7), we obtain,

$$2R_0 W = e^{-\delta\theta}\frac{d^2 U}{d\eta^2} - \delta e^{-\delta\theta}\frac{d\theta}{d\eta}\frac{dU}{d\eta} - \frac{M(U - \lambda + mW)}{(1 + m^2)} \tag{9}$$

$$-2Ro(U - \lambda) = e^{-\delta\theta}\frac{d^2 W}{d\eta^2} - \delta e^{-\delta\theta}\frac{d\theta}{d\eta}\frac{dW}{d\eta} - \frac{M(W - mU + m\lambda))}{(1 + m^2)} \tag{10}$$

$$\frac{d^2\theta}{d\eta^2} + \Pr Ec\left[\left(\frac{dU}{d\eta}\right)^2 + \left(\frac{dW}{d\eta}\right)^2\right]e^{-\delta\theta} + \Pr EcM\left[\frac{(U - \lambda + mW)^2 + (W - mU + m\lambda)^2}{(1 + m^2)^2}\right] = 0 \tag{11}$$

$$Ns = \left(\frac{d\theta}{d\eta}\right)^2 + Br\left[\left(\frac{dU}{d\eta}\right)^2 + \left(\frac{dW}{d\eta}\right)^2\right]e^{-\delta\theta} + BrM\left[\frac{(U - \lambda + mW)^2 + (W - mU + m\lambda)^2}{(1 + m^2)^2}\right] \tag{12}$$

with

$$U(0) = 0, \quad W(0) = 0, \quad \theta(0) = 0,$$
$$U(1) = \lambda, \quad W(1) = 0, \quad \theta(1) = 0, \tag{13}$$

where Pr is the Prandtl number, R_0 is the rotation parameter, Ec is the Eckert number, δ is the viscosity variation parameter, M is the magnetic field parameter, Br $(=EcPr)$ is the Brinkm ann number and λ is the upper wall motion parameter. Other quantities of interest are the skin friction coefficients $(Cf_1$ and $Cf_2)$, Nusselt number (Nu) and the Bejan number (Be) which are given as

$$Cf_1 = \frac{L^2 \tau_1}{\rho \upsilon^2} = e^{-\delta\theta} \left. \frac{dU}{d\eta} \right|_{\eta=0,1}, \quad Cf_2 = \frac{L^2 \tau_2}{\rho \upsilon^2} = e^{-\delta\theta} \left. \frac{dW}{d\eta} \right|_{\eta=0,1},$$

$$Nu = -\frac{L q_m}{k(T_1 - T_0)} = -\left. \frac{d\theta}{d\eta} \right|_{\eta=0,1}, \quad Be = \frac{N_1}{Ns} = \frac{1}{1+\varphi} \tag{14}$$

where

$$\tau_1 = \mu \frac{\partial u}{\partial y}, \quad \tau_2 = \mu \frac{\partial w}{\partial y}, \quad q_m = -k \frac{\partial T}{\partial y}, N_1 = \left(\frac{d\theta}{d\eta} \right)^2, \varphi = \frac{N_2}{N_1},$$

$$N_2 = Br e^{-\delta\theta} \left[\left(\frac{dU}{d\eta} \right)^2 + \left(\frac{dW}{d\eta} \right)^2 \right] + Br M \left[\frac{(U - \lambda + mW)^2 + (W - mU + m\lambda)^2}{(1+m^2)^2} \right] \tag{15}$$

It is very important to note that N_1 represents the thermodynamic irreversibility due to heat transfer while N_2 corresponds to the combined effects of fluid friction and magnetic field irreversibility. When $Be = 0.5$ both N_1 and N_2 contribute equally to the entropy generation in the flow process. The model Equations (9)–(14) are tackled numerically using a shooting technique coupled with fourth order Runge–Kutta–Fehlberg integration scheme.

3. Numerical Procedure

Here, the nonlinear model governing Equations (9)–(11) together with the Boundary Conditions (13) represent a boundary value problem (BVP) and are converted into a set of nonlinear first order ordinary differential equations with some unknown initial conditions that are determined using shooting technique. Let,

$$U = y_1, U' = y_2, W = y_3, W' = y_4, \theta = y_5, \theta' = y_6. \tag{16}$$

Hence, the governing equations become:

$$\left. \begin{aligned} y_1' &= y_2, \quad y_2' = \delta y_6 y_2 + e^{\delta y_5} \left(2R_0 y_3 + \frac{M(y_1 - \lambda + my_3)}{(1+m^2)} \right), \\ y_3' &= y_4, \quad y_4' = \delta y_6 y_4 + e^{\delta y_5} \left(\frac{M(y_3 - my_1 + m\lambda)}{(1+m^2)} - 2R_0(y_1 - \lambda) \right) \\ y_5' &= y_6, \quad y_6' = -\Pr Ec \left(y_2^2 + y_3^2 \right) e^{-\delta y_5} - \Pr Ec M \left[\frac{(y_1 - \lambda + my_3)^2 + (y_3 - my_1 + m\lambda)^2}{(1+m^2)^2} \right] \end{aligned} \right\} \tag{17}$$

with the corresponding initial conditions as

$$y_1(0) = 0, \quad y_2(0) = s_1, \quad y_3(0) = 0, \quad y_4(0) = s_2, \quad y_5(0) = 0, \quad y_6(0) = s_3. \tag{18}$$

The unknown initial conditions s_1, s_2, and s_3 are first guessed and subsequently determined using Newton–Raphson's method for each set of parameter values with respect to the prescribed boundary conditions. The resulting initial value problem is tackled numerically using a fourth order Runge–Kutta–Fehlberg integration scheme. The step size $\eta = 0.01$ for the numerical solution. From the process of numerical computation, we obtain the skin friction coefficients (Cf_1 and Cf_2), the Nusselt number (Nu), the entropy generation rate and the Bejan number as given by Equation (14).

4. Results and Discussion

In order to have a physical insight of the problem, we discuss the effects of various thermophysical parameters controlling the flow system displayed in Figures 2–9. Figure 2 depicts the primary velocity profiles in the x-direction. It is zero at the fixed lower wall and increasing gradually with the maximum velocity at the upper moving wall satisfying the prescribed boundary conditions. In Figure 2a, it is observed that the primary velocity profiles rises towards the lower fixed wall with an increase in magnetic field intensity (M). This may be due to the combined actions of Lorenz force and the moving upper wall. Figure 2b depicts the effect of increasing in upper wall motion parameter (λ). As λ is increasing, the fluid primary velocity generally increases across the channel with maximum primary velocity at the upper wall. Figure 2c,d shows the effect of increase in rotation parameter (R_0) and the viscosity variation parameter (δ). An increase in each of these parameters produces a rise in the primary velocity profile across the channel and towards the upper wall. This may be attributed to the facts that as δ increases, the fluid viscosity decreases leading to an increase its primary velocity. In Figure 2e, it is observed that as Hall current parameter (m) increases, the fluid primary velocity decreases across the channel. Meanwhile, an increase in viscous heating also increases the primary velocity profiles as illustrated in Figure 2f. Figure 3 shows the effects of parameter variation on fluid secondary velocity profiles in z-direction. It is interesting to note that a general flow reversal is observed. Moreover, the intensity of flow reversal along z-direction decreases with a boost in magnetic field but increases with increasing parameter values of λ, m and Ec. Figure 4 demonstrates the response of fluid temperature profiles to parameter variation. It is noteworthy that the temperature profile is parabolic with maximum value within the channel core region. The fluid temperature rises with increasing parameter values of M, R_0, Ec and λ but decreasing with increasing parameter values of m and δ. Figure 5 depicts the effects of thermophysical parameters on the entropy generation rate. Generally, the entropy production is highest at the lower fixed wall and lowest at the upper moving wall. This can be attributed to the fact that high velocity and temperature gradients are experienced at the lower fixed wall as compared to the upper moving wall. Moreover, it is interesting to note that entropy generation rate further increases at the lower fixed wall and decreases at the upper moving wall with increasing parameter values of M and R_0 as shown in Figure 5a,c. At the point $(\eta = 0.5)$, increase in M and R_0 does not affect entropy generation rate while at the point $(\eta = 0.5)$. Meanwhile, an increase in the upper wall motion generally increases entropy generation across the channel while a decrease in the fluid viscosity (*i.e.*, δ increases) decreases the entropy production rate (see Figure 5b,d).

In Figure 5e, we observed that entropy production at the lower wall decreases while that at the upper wall increases with increasing Hall parameter. At the point $\eta = 0.6$, increase in m does not affect entropy generation rate. An increase in Eckert number due to fluid friction also increases the entropy generation rate across the channel as depicted in Figure 5f. Figure 6 depicts the effects of increasing parameters on Bejan number. A point exists at $\eta = 0.4$ where the fluid friction and magnetic field irreversibility completely dominates the entire flow system. Figure 6a shows that the Bejan number at both lower and upper walls increases as M increases but decreases within the region $0.1 < \eta < 0.4$. This implies that the thermodynamic irreversibility due to heat transfer dominates the flow at both walls; however, within the region $0.1 < \eta < 0.4$, the combined effects of fluid friction and magnetic field irreversibility dominate. Figure 6b,f shows that Bejan number increases at both walls with increasing values of λ and Ec, this implies irreversibility due to heat transfer is enhanced. Figure 6c,d shows that the Bejan number decreases at lower wall region but increases at upper wall region with increasing R_0 and δ. This shows that an increase in the fluid rotation coupled with a decrease in viscosity with enhance fluid friction irreversibility at the lower wall region and the heat transfer irreversibility at the upper wall region. Figure 6e shows that Bejan number increases at lower wall region and decreases at upper wall region with an increase in Hall current intensity (m). Figure 7 illustrates the effects of parameter variation of Nusselt number both at the lower fixed wall and the upper moving wall. It is observed that the heat transfer rate is generally higher at the lower fixed wall as compared to that of upper moving wall. Moreover, an increase in λ and R_0 increases heat transfer rate due to the elevation in temperature gradient at the walls while an increase in δ decreases wall heat flux. The skin frictions at both walls with respect to primary and secondary flow velocity gradients are depicted in Figure 8. It is observed that the skin friction in the z-direction due the secondary flow velocity gradient is higher at the lower wall as compared to that of the upper wall as shown in Figure 8. An increase in λ, m and R_0 increases the secondary flow skin friction while an increase in magnetic field intensity parameter M decreases the secondary flow skin friction. It is interesting to note that the secondary flow skin friction decreases at the lower fixed wall and increases at the upper moving wall with a decrease in fluid viscosity (*i.e.*, δ increases). Figure 9 shows that the primary flow skin friction in the x-direction is higher at the upper moving wall as compared to that of lower fixed wall. Moreover, the primary flow skin friction increases at the lower wall but decreases at the upper wall with an increase in the intensity of R_0 and M. The trend is opposite with increasing parameter values of m and δ. An increase in the upper wall motion λ increases the primary flow skin friction at both lower and upper walls.
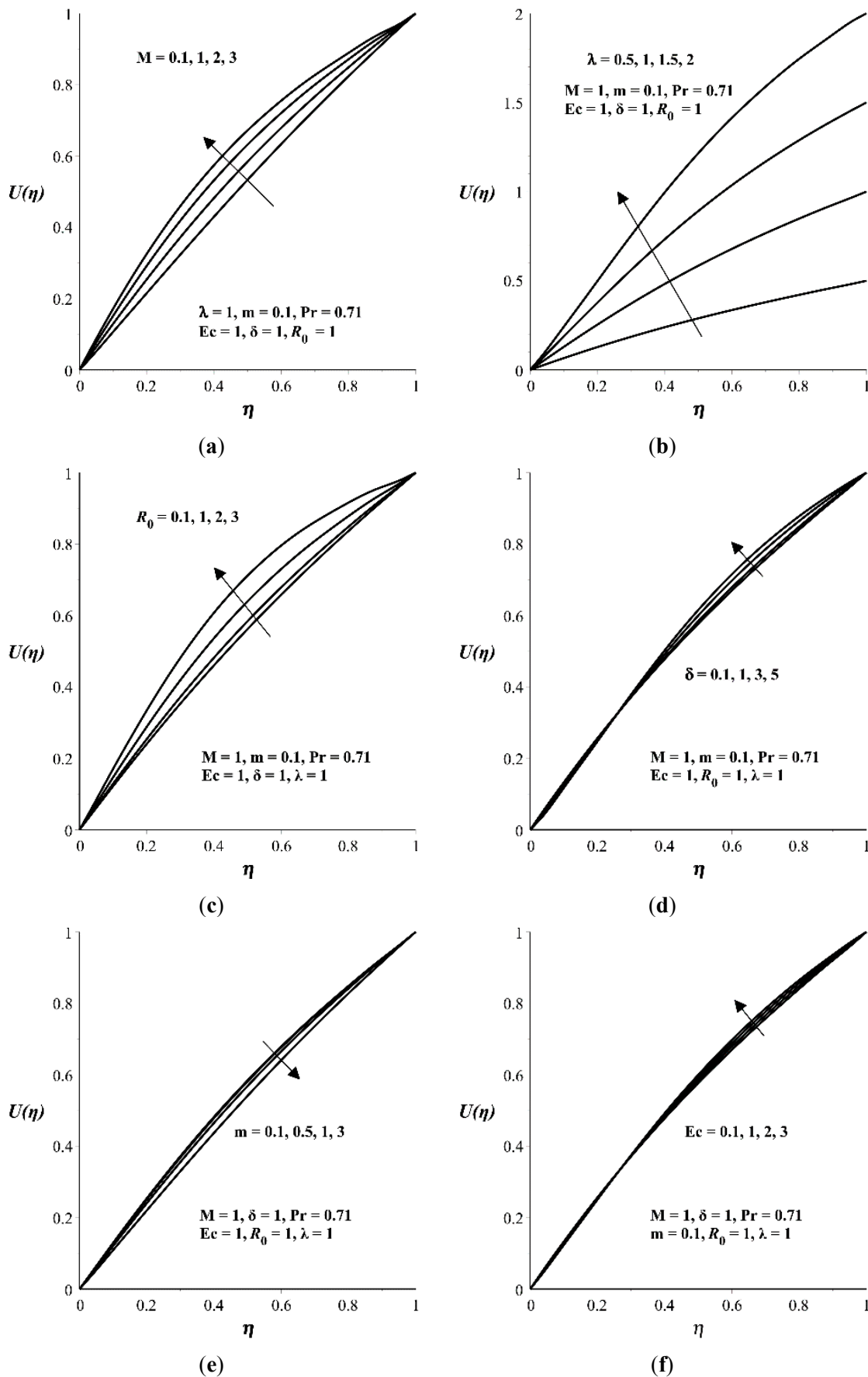
Figure 2. Velocity profile in *x*-direction with increasing (**a**) *M*, (**b**) λ, (**c**) R_0, (**d**) δ, (**e**) *m*, and (**f**) *Ec*.
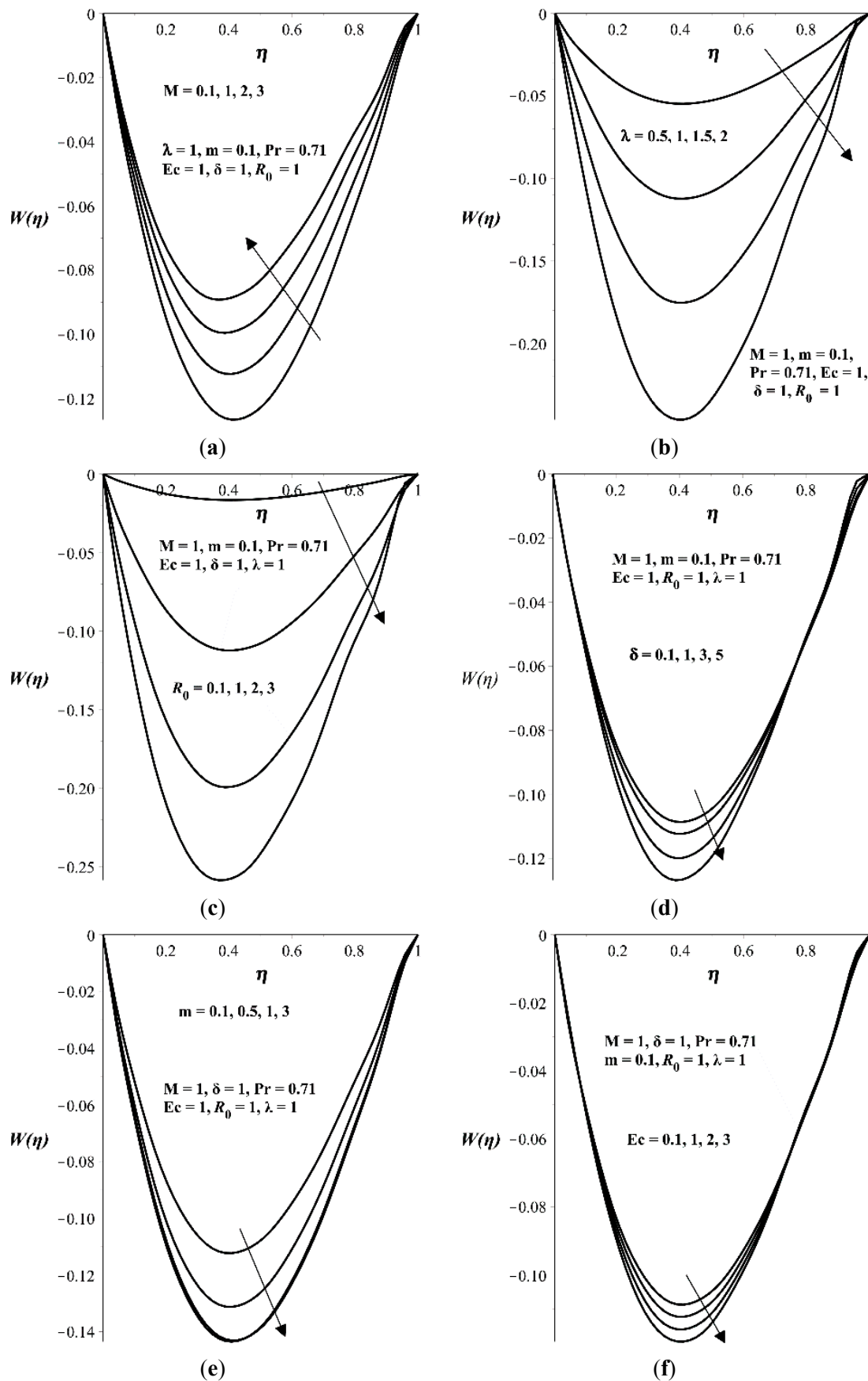
Figure 3. Velocity profile in z-direction with increasing (**a**) *M*, (**b**) λ, (**c**) R_0, (**d**) δ, (**e**) *m*, and (**f**) *Ec*.
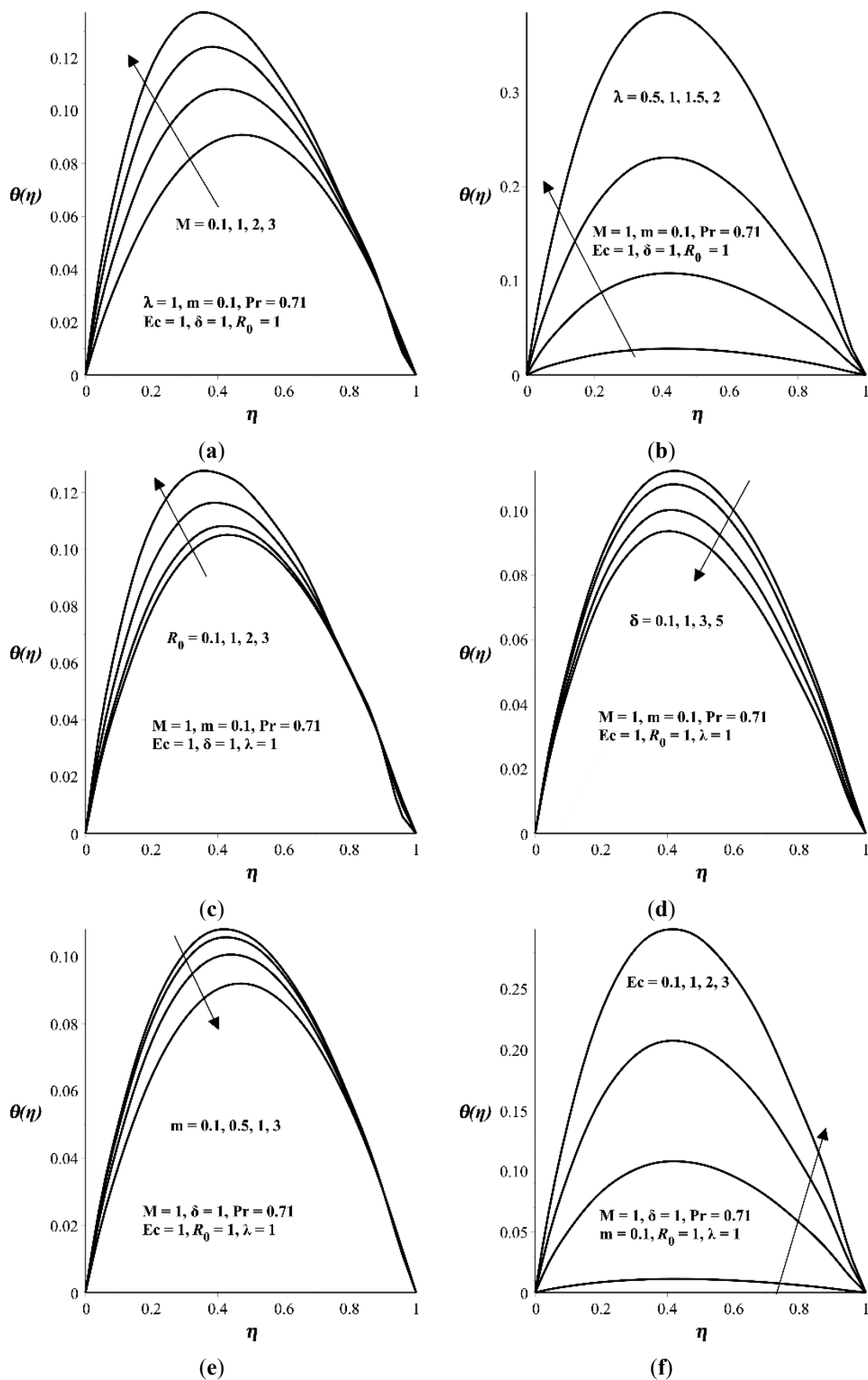
Figure 4. Temperature profile with increasing (**a**) *M*, (**b**) λ, (**c**) R_0, (**d**) δ, (**e**) *m*, and (**f**) *Ec*.
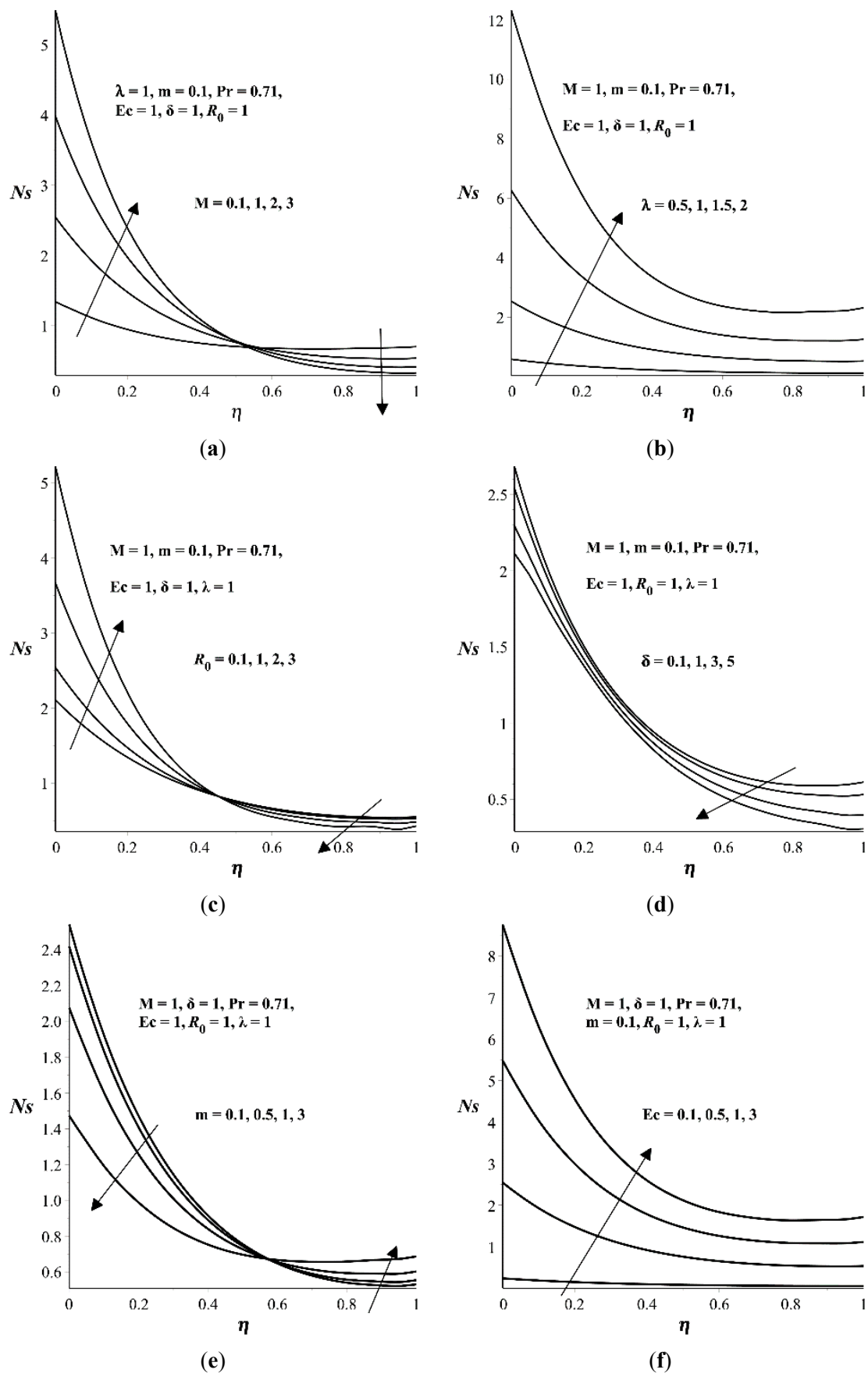
Figure 5. Entropy generation with increasing (**a**) *M*, (**b**) λ, (**c**) R_0, (**d**) δ, (**e**) *m*, and (**f**) *Ec*.
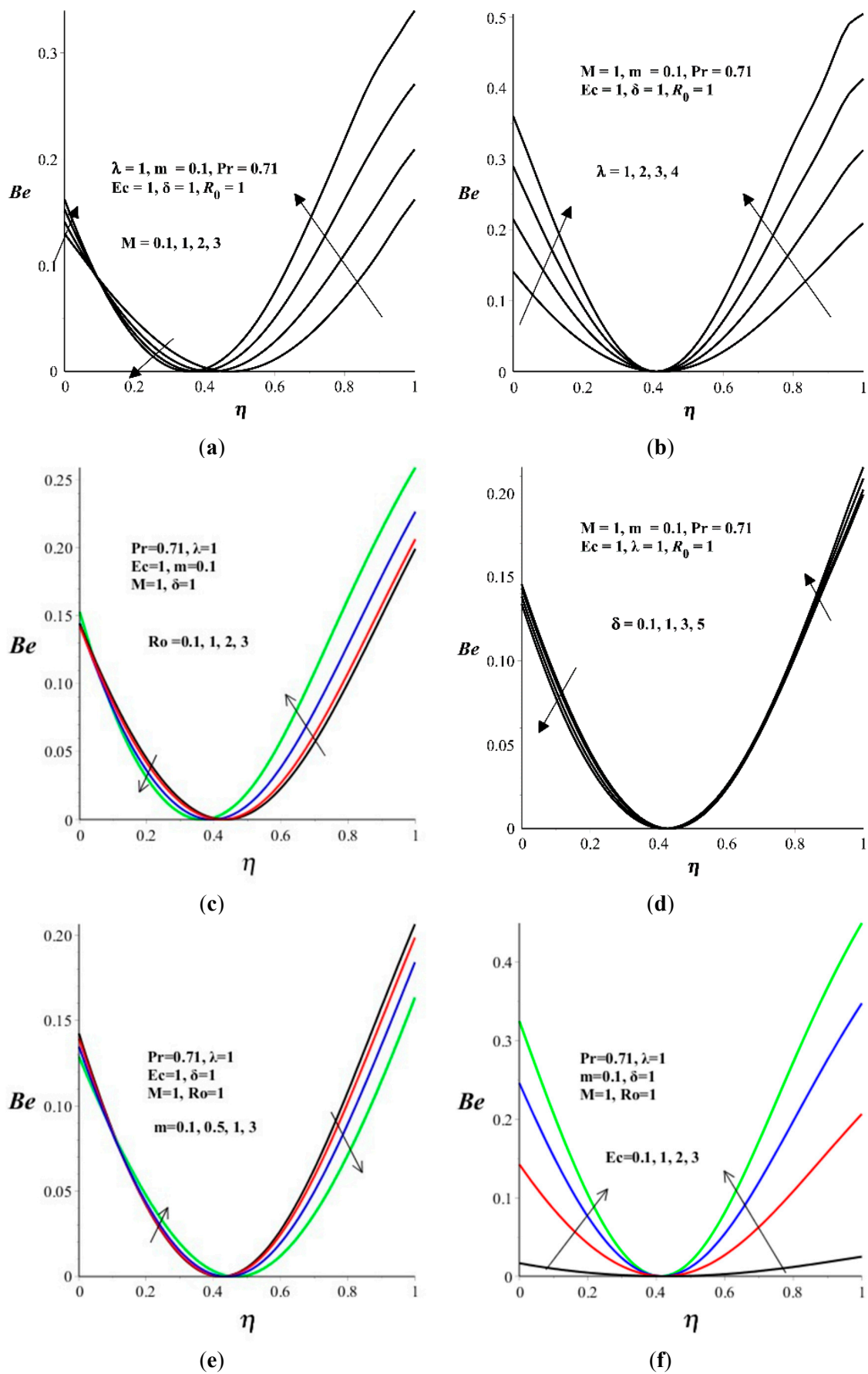
Figure 6. Benja number with increasing (**a**) *M*, (**b**) λ, (**c**) R_0, (**d**) δ, (**e**) *m*, and (**f**) *Ec*.
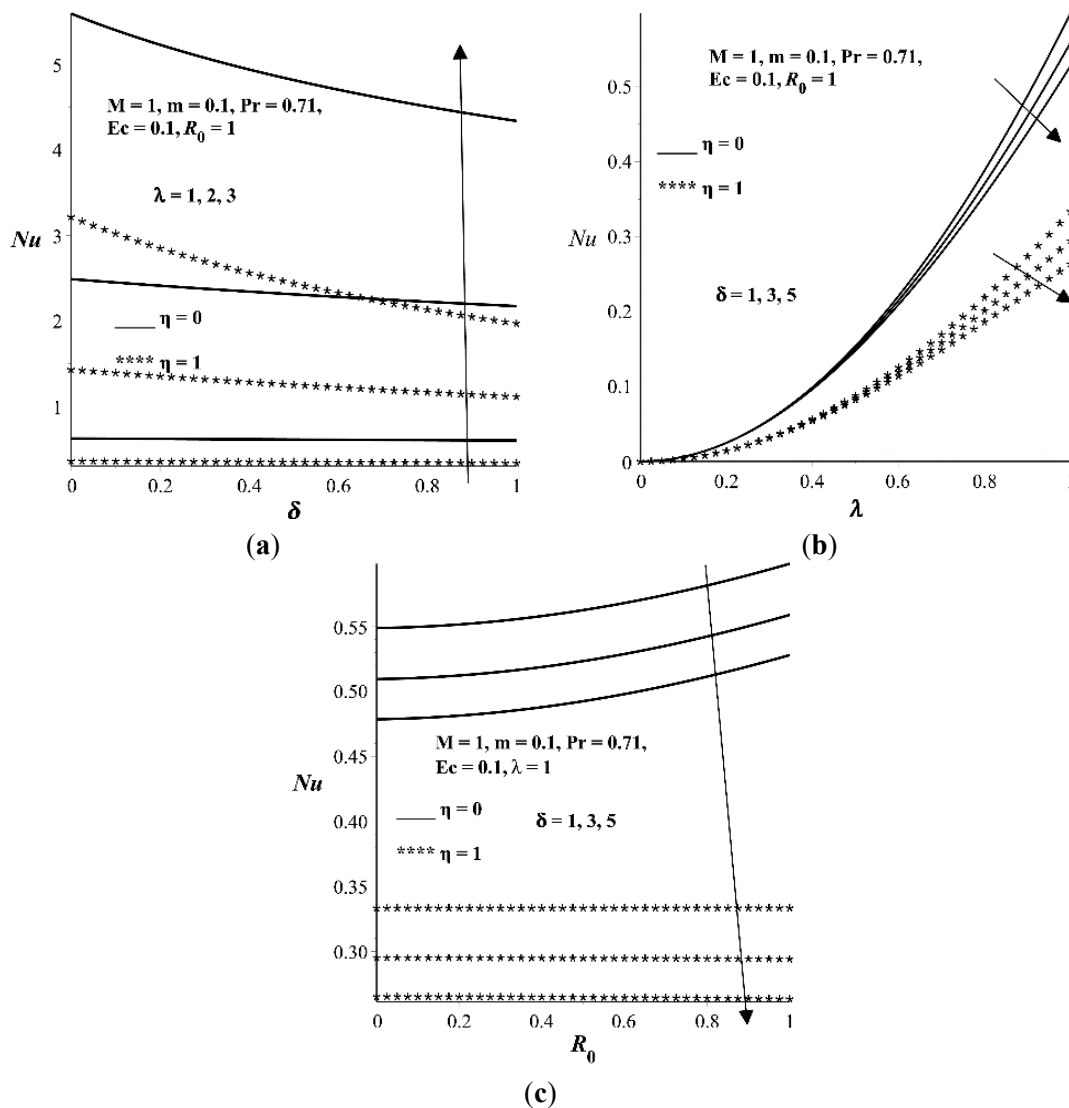
Figure 7. Nusselt number with increasing (**a**) λ *versus* δ , (**b**) δ *versus* λ , and (**c**) δ *versus* R_0 .
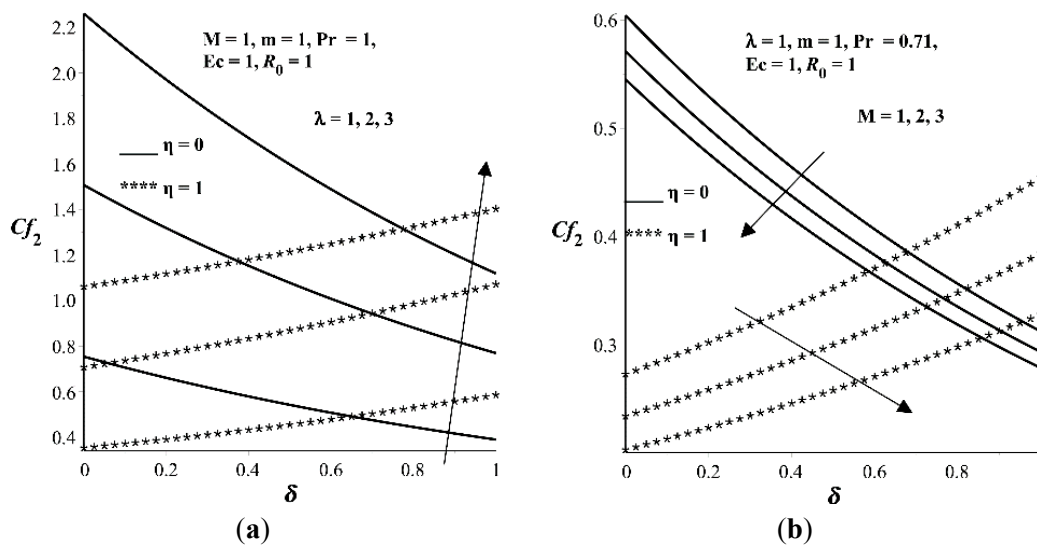
Figure 8. *Cont.*
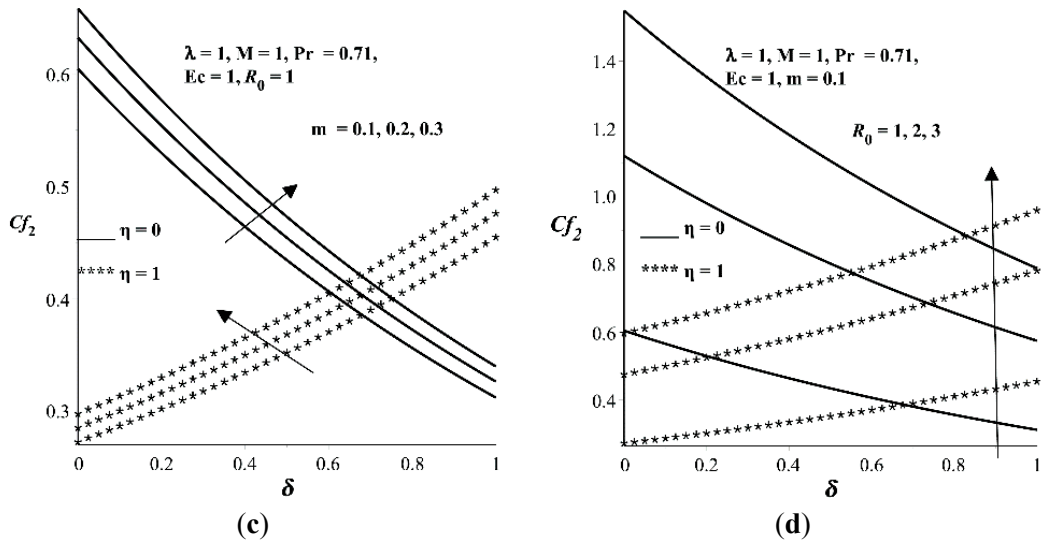
Figure 8. Cf_2 with increasing (**a**) λ *versus* δ, (**b**) M *versus* δ, (**c**) m *versus* δ, and (**d**) R_0 *versus* δ.
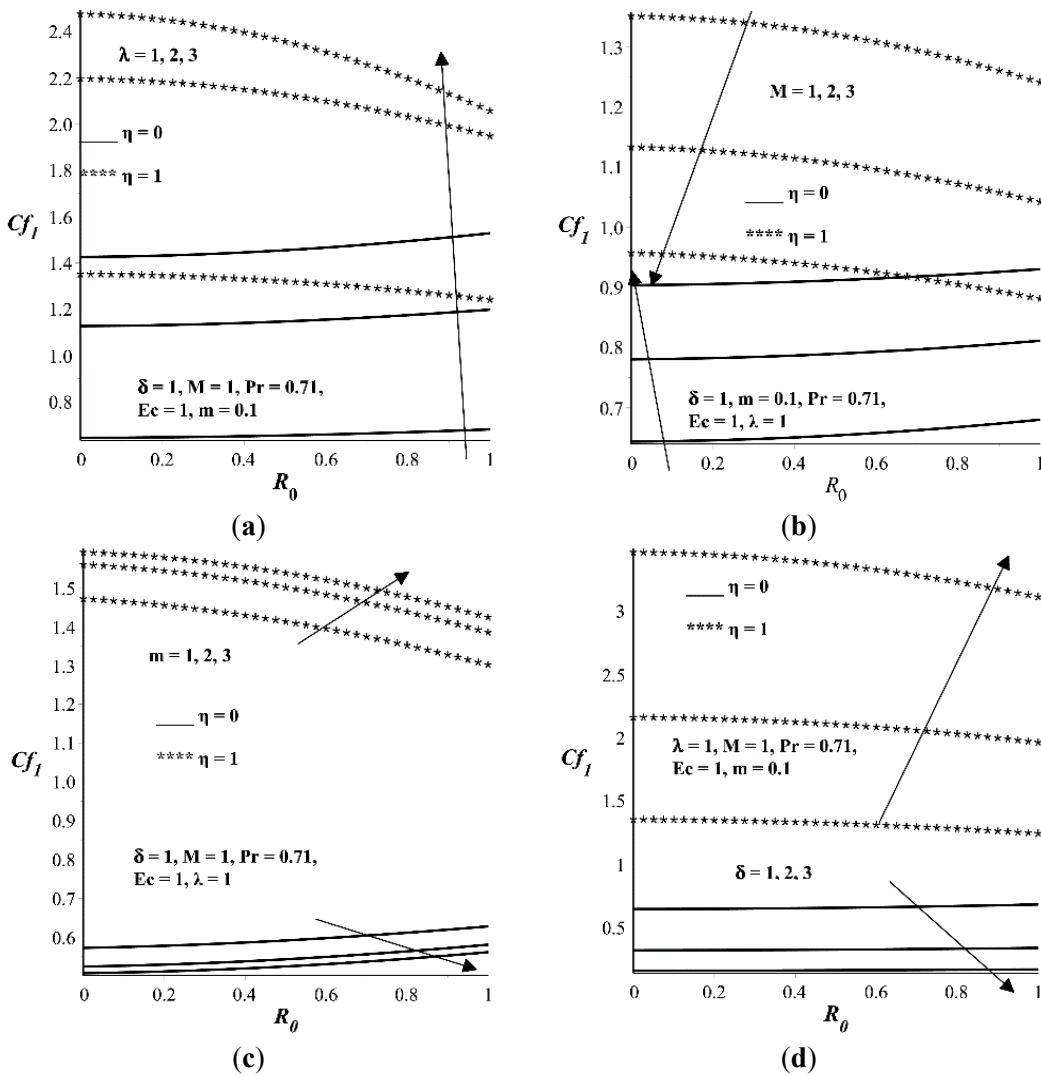
Figure 9. Cf_1 with increasing (**a**) λ *versus* R_0, (**b**) M *versus* R_0, (**c**) m *versus* R_0, and (**d**) δ *versus* R_0.

5. Conclusions

The thermodynamic analysis of variable viscosity hydromagnetic Couette flow in a rotating system with Hall current is investigated. The nonlinear model is tackled numerically using shooting technique coupled with fourth order Runge–Kutta–Fehlberg integration scheme. Our results can be summarized as follows:

- The primary velocity profiles in *x*-direction increases with M, λ, R_0, and δ but decreases with *m*.
- The secondary velocity profiles in *z*-direction increases with M but decreases with λ, R_0, δ and *m*.
- The temperature profile increases with M, λ, R_0, and *Ec* but decreases with m and δ.
- The entropy generation rate increases with λ and *Ec* but decreases with δ.
- Heat transfer irreversibility is more at the upper moving wall as compared to lower fixed wall. A point exists at $\eta = 0.4$ where the fluid friction and magnetic field irreversibility completely dominate the flow system. The Bejan number increases with λ and *Ec*.
- The Nusselt number is higher at the lower wall as compared to upper wall. An increase in λ and R_0 increases Nu while an increase in δ decreases Nu.
- The secondary flow skin friction coefficient increases with λ, *m*, and R_0 but decreases with *M*.
- Increase in R_0 and *M* increases the primary flow skin friction coefficient at the lower wall but decreases it at the upper wall. The trend is opposite with increasing parameter values of *m* and δ. An increase in λ increases the primary flow skin friction at both lower and upper walls.

Acknowledgments

Author Contributions

The authors contributed equally to this work. All authors have read and approved the final manuscript.

Conflicts of Interest

The authors declare no conflict of interest.

References

1. Barikbin, Z.; Ellahi, R.; Abbasbandy, S. The Ritz–Galerkin method for MHD Couette flow of non-Newtonian fluid. *Int. J. Ind. Math.* **2014**, *6*, 235–243.
2. Khan, A.A.; Ellahi, R.; Usman, M. The effects of variable viscosity on the flow of non-Newtonian fluid through a porous medium in an inclined channel with slip conditions. *J. Porous Media* **2013**, *16*, 59–67.
3. Rashad, A.M. Effects of radiation and variable viscosity on unsteady MHD flow of a rotating fluid from stretching surface in porous medium. *J. Egypt. Math. Soc.* **2014**, *22*, 134–142.

4. Torabi, M.; Zhang, K. First and second thermodynamic laws analyses between and inside two rotating solid cylindrical geometries with magnetohydrodynamic flow. *Int. J. Heat Mass Transf.* **2015**, *89*, 760–769.

5. Hayat, T.; Nadeem, S.; Siddiqui, A.M.; Asqhar, S. An oscillating hydromagnetic non-Newtonian flow in a rotating system. *Appl. Math. Lett.* **2004**, *17*, 609–614.

6. Eegunjobi, A.S.; Makinde, O.D. Second law analysis for MHD permeable channel flow with variable electrical conductivity and asymmetric Navier slips. *Open Phys.* **2015**, *13*, 100–110.

7. Attia, H.A. Effect of Hall current on transient hydromagnetic Couette–Poiseuille flow of a viscoelastic fluid with heat transfer. *Appl. Math. Model.* **2008**, *32*, 375–388.

8. Makinde, O.D.; Chinyoka, T. Numerical study of unsteady hydromagnetic Generalized Couette flow of a reactive third-grade fluid with asymmetric convective cooling. *Comput. Math. Appl.* **2011**, *61*, 1167–1179.

9. Eegunjobi, A.S.; Makinde, O.D. Entropy Generation Analysis in a Variable Viscosity MHD Channel Flow with Permeable Walls and Convective Heating. *Math. Probl. Eng.* **2013**, *2013*, doi:10.1155/2013/630798.

10. Shivakumara, I.S.; Lee, J.; Vajravelu, K.; Akkanagamma, M. Electrothermal convection in a rotating dielectric fluid layer: Effect of velocity and temperature boundary conditions. *Int. J. Heat Mass Transf.* **2012**, *55*, 2984–2991.

11. Nadeem, S.; Saleem, S. Analytical study of third grade fluid over a rotating vertical cone in the presence of nanoparticles. *Int. J. Heat Mass Transf.* **2015**, *85*, 1041–1048.

12. Turkyilmazoglu, M. Exact solutions for the incompressible viscous magnetohydrodynamic fluid of a porous rotating disk flow with Hall current. *Int. J. Mech. Sci.* **2012**, *56*, 86–95.

13. Zakinyan, A.; Nechaeva, O.; Dikansky, Y. Motion of a deformable drop of magnetic fluid on a solid surface in a rotating magnetic field. *Exp. Therm. Fluid Sci.* **2012**, *39*, 265–268.

14. Feiz-Dizaji, A.; Salimpour, M.R.; Jam, F. Flow field of a third-grade non-Newtonian fluid in the annulus of rotating concentric cylinders in the presence of magnetic field. *J. Math. Anal. Appl.* **2008**, *337*, 632–645.

15. Hayat, T.; Khan, L.A.; Ellahi, R.; Obaidat, S. Exact solutions on MHD flow past an accelerated porous plate in a rotating frame. *Chin. Phys. Lett.* **2011**, *28*, doi:10.1088/0256-307X/28/5/054701.

16. Batista, M. Steady flow of incompressible fluid between two co-rotating disks. *Appl. Math. Model.* **2011**, *35*, 5225–5233.

17. Singh, A.K.; Singh, N.P.; Singh, U.; Singh, H. Convective flow past an accelerated porous plate in rotating system in presence of magnetic field. *Int. J. Heat Mass Transf.* **2009**, *52*, 3390–3395.

18. Malashetty, M.S.; Swamy, M.S.; Sidram, W. Thermal convection in a rotating viscoelastic fluid saturated porous layer. *Int. J. Heat Mass Transf.* **2010**, *53*, 5747–5756.